https://doi.org/10.5194/wes-2019-62
Preprint. Discussion started: 5 September 2019

eawe european academy of wind energy
Open Access WIND ENERGY SCIENCE DISCUSSIONS

Ducted wind turbines in yawed flow: A numerical study

Vinit Dighe[1], Dhruv Suri[2], Francesco Avallone[1], and Gerard van Bussel[1]

[1]Wind Energy Research Group, Faculty of Aerospace Engineering, Technological University of Delft, Netherlands
[2]Renewable Energy Research Group, Department of Aeronautical and Automobile Engineering, Manipal Institute of Technology, India

Correspondence: Vinit Dighe (v.v.dighe@tudelft.nl)

Abstract. Ducted Wind Turbines (DWTs) can be used for energy harvesting in urban areas where non-uniform flows are caused by the presence of buildings or other surface discontinuities. For this reason, the aerodynamic performance of DWTs in yawed flow conditions must be characterized. A numerical study to investigate the characteristics of flow around two DWT configurations using a simplified duct-actuator disc (AD) model is carried out. The analysis shows that the aerodynamic performance of a DWT in yawed flow is dependent on the mutual interaction between the duct and the rotor; an interaction that changes with duct geometry, AD loading and operating conditions. It is found that the duct cross-section camber not only offers insensitivity to yaw, but also a gain in performance up to a specific yaw angle; thereafter any further increase of yaw results in a performance drop.

1 Introduction

Global energy demand is expected to more than double by 2050 owing to the growth in population and economies (Gielen et al., 2019). The global wind power capacity quadrupled in less than a decade, reaching 597 Gigawatt by the end of 2018 compared to 120 Gigawatt in 2008 (Dupont et al., 2018). Wind turbines are typically installed away from the populated areas considering the enforced visual and noise regulations. This necessitates the transfer of electricity via grids over larger distances, which increases the levelized cost of electricity (LCOE). Integration of wind turbines into urban areas is challenging. The presence of buildings, trees and surface discontinuities in urban areas lead to lower wind speed, non-uniform inflow and larger turbulent fluctuations compared to open fields. To address these challenges, design modifications of wind turbines, suitable for operation in an urban setting, is required.

A possible technological solution to extract wind energy in urban areas are Ducted Wind Turbines (DWTs). DWTs increase the energy extraction with respect to conventional horizontal axis wind turbines (HAWTs) for a given rotor radius and free-stream velocity (van Bussel, 2007). DWTs are constituted of a rotor and a duct (also named as diffuser or shroud); the role of the latter is to increase the flow rate through the rotor relative to a similar rotor operating in the open atmosphere; thereby increasing the generated power. There are more than one explanations for how this to occur. One explanation is that the duct forces an expansion of flow downstream of the turbine beyond what is attainable for a bare wind turbine. This provides a reduced pressure behind the turbine, and increase the total mass flow through the turbine (van Bussel, 2007). A second explanation, as argued by de Vries (1979), is that if the sectional lift force of the duct is directed towards the turbine plane, then the associated circulation

https://doi.org/10.5194/wes-2019-62
Preprint. Discussion started: 5 September 2019

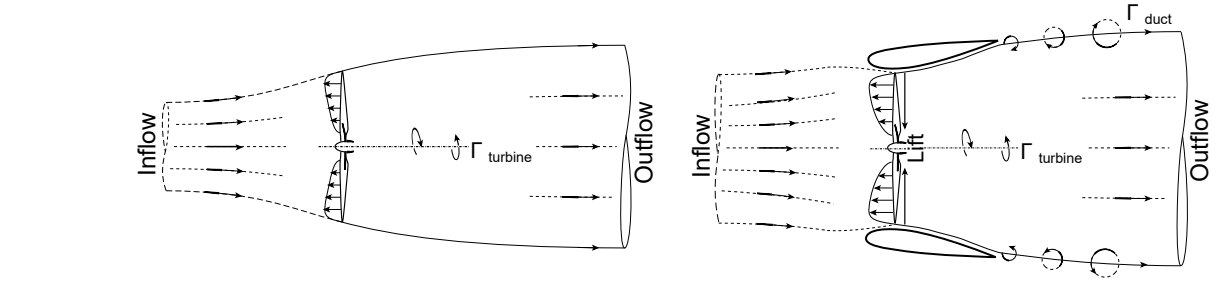

Figure 1. Schematic of stream-tube model for a bare turbine (left) and DWT (right). The bound circulation from the turbine blades and the duct surface is denoted by τ

(see Figure 1) of the duct increases the mass flow through the turbine. A significant amount of literature on DWTs, based on the combined use of theoretical, numerical and experimental techniques, exists (Igra, 1981; Gilbert and Foreman, 1983; Abe et al., 2005; Toshimitsu et al., 2008; Werle and Presz, 2008; Khamlaj and Rumpfkeil, 2017). Questions over the performance of DWTs in yawed flow remain, however.

Igra (1981) studied experimentally the effects of yaw on the performance of DWTs. Eight geometries, with different duct configurations and an actuator disc (AD) representing the turbine, were investigated using simplified duct-AD models. He found that the total thrust of the duct-AD system increases with increasing yaw angle up to a specific angle; thereafter any further increase of yaw angle results in thrust reduction. On the other hand, using a slotted duct, the total thrust of the duct-AD system decreases with increasing yaw angle. Phillips et al. (2002) combined experimental and numerical analysis to study DWT under yawed flow. In contrast to the previous study, they concluded that the thrust increase for a DWT in yawed flow is due to the slotted design of the duct, with the added mass flow of air through the slot increasing the boundary layer flow control and preventing separation over the suction side (inner surface) of the duct

The above literature, due to the contrasting nature of the conclusions, lacks clarity on the aerodynamics of DWTs in yawed flow. The goal of the present paper is to characterize the effects of yaw on the aerodynamic performance of DWTs. This is performed using URANS CFD approach. To this aim, two reference duct geometries are selected and the rotor is simulated by a uniformly loaded AD model (Dighe et al., 2018).

The rest of the paper is organized as follows. Section 2 reports the non-dimensional coefficients adopted for characterizing the aerodynamic performance of the duct-AD model, both under non-yawed and yawed flow conditions. Section 3 describes the computational settings and parameters with a brief description of the numerical methodology. Section 4 reports the validation of the numerical method with the experimental data. Insights on the aerodynamic performance coefficients with respect to yawed flow will be discussed in section 5, together with flow analysis. Finally, the most relevant results are summarized in the conclusions.

https://doi.org/10.5194/wes-2019-62
Preprint. Discussion started: 5 September 2019

eawe european academy of wind energy
Open Access WIND ENERGY SCIENCE DISCUSSIONS

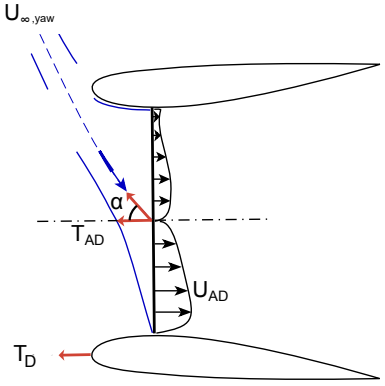

Figure 2. Schematic of yawed flow around a duct-AD model

2 Duct - AD flow model

The turbine is modelled by a flat AD of infinitesimal width. The AD exerts a constant thrust force, calculated across the AD surface S_{AD}, which corresponds to a non-dimensional thrust force coefficient:

$$C_{T,AD} = \frac{T_{AD}}{\frac{1}{2}\rho {U_\infty}^2 S_{AD}}, \tag{1}$$

where ρ is the fluid density and U_∞ is the free-stream velocity.

To generate T_{AD}, a uniform pressure drop is present across the AD surface, $T_{AD} = \Delta p \times S_{AD}$. The pressure drop Δp is taken from experiments (Tang and van Bussel, 2018) and is given as an input parameter to the numerical simulations. The mean velocity across the AD radial plane, which is a uni-variate function of AD thrust coefficient: $U_{AD_0} = f(C_{T,AD})$, can be expressed by integrating the difference of the free-stream velocity component U_x across the AD surface:

$$\frac{U_{AD_0}}{U_\infty} = \frac{1}{S_{AD}} \oint_{S_{AD}} U_x dS. \tag{2}$$

Using Eqs. 1 and 2, the power coefficient for a bare AD reads:

$$C_{P_o} = \frac{U_{AD_0}}{U_\infty} C_{T,AD}. \tag{3}$$

The subscript 0 has been adopted for quantities evaluated for bare AD configuration.

For a duct-AD configuration, an additional thrust force exerted by the duct on the flow, or vice-versa, appears. Then, the total thrust force T is the vectorial sum of the AD thrust force T_{AD}, and the duct thrust force T_D, given by:

$$T = T_{AD} + T_D. \tag{4}$$

The total thrust coefficient is then defined as:

$$C_T = C_{T,AD} + C_{T,D}. \tag{5}$$

https://doi.org/10.5194/wes-2019-62
Preprint. Discussion started: 5 September 2019

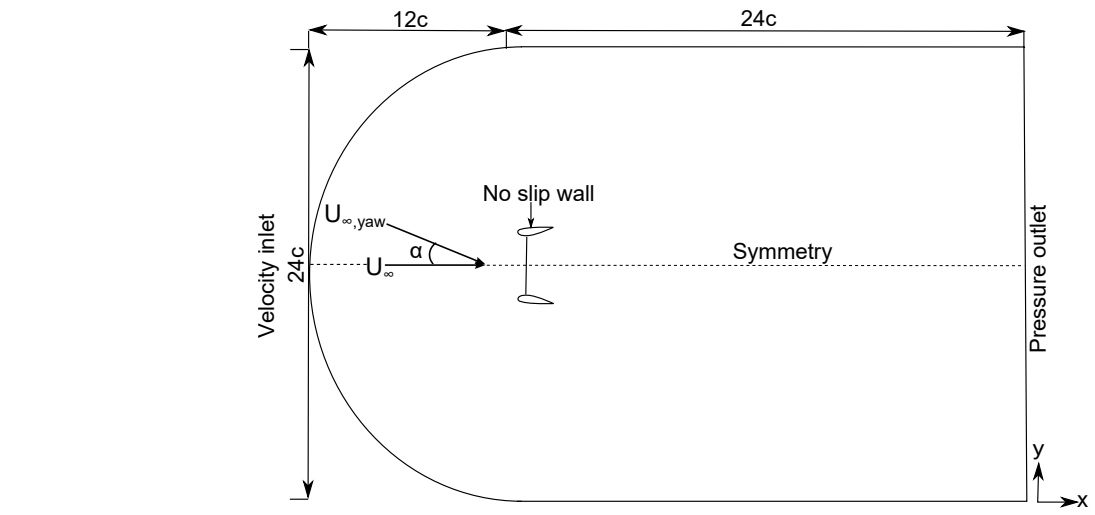

Figure 3. Computational domain showing the boundary conditions employed. The lengths are normalized with the duct chord length c. Representative, not to scale.

Note that the duct thrust coefficient $C_{T,D}$ is normalized with the AD area S_{AD} to facilitate direct addition to the AD thrust coefficient $C_{T,AD}$ for calculating the total thrust coefficient C_T. Then, the mean velocity at the AD for a duct-AD model is a bivariate function of AD thrust coefficient and the duct thrust coefficient: $U_{AD} = f(C_{T,AD} + C_{T,D}) = f(C_T)$. Similar to Eq. 3, the power coefficient for the duct-AD model, using S_{AD} as the reference area, becomes:

$$C_P = \frac{U_{AD}}{U_\infty} C_T. \tag{6}$$

The power coefficient expression in Eq. 6 challenges the well-known Lanchester–Betz–Joukowsky limit of $\frac{16}{27}$ for maximum power coefficient obtainable for a HAWT. This should not appear like a surprising result, since, the mass flow of air swallowed in the presence of duct is greater due to the additional thrust force $C_{T,D}$ offered by the duct. The above relations are also valid for the DWT under yawed flow condition. Figure 2 shows the schematic of flow around the duct-AD model, where α is the yaw angle relative to the incident free-stream direction. Thus, in practice, if $C_{T,D} > 0$, then a higher power coefficient can be obtained for a DWT in comparison to a HAWT with the same rotor (Bontempo and Manna, 2013).

3 Numerical approach

A commercial CFD solver ANSYS Fluent® has been used for a complete viscous transient solution of incompressible flow around the duct-AD model. The governing flow equations are the Unsteady Reynolds-averaged Navier Stokes (URANS) equations. The 2D computational domain is shown in Figure 3, where the distance from the AD location to the domain inlet and outlet are $12c$ and $24c$, respectively. For the present computations, a C-grid structured zonal approach is chosen, see Figure 4, which proved advantageous in the case of a curved boundary, i.e. duct's leading edge. The C-shaped loop terminates in

https://doi.org/10.5194/wes-2019-62
Preprint. Discussion started: 5 September 2019

eawe european academy of wind energy
Open Access WIND ENERGY SCIENCE DISCUSSIONS

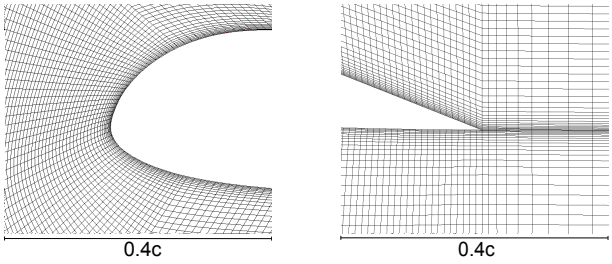

Figure 4. Computational grid surrounding the leading and trailing edge of the duct

Table 1. Grid statistics for grid independence study of the reference case.

Grid	Number of cells	$C_{T,D}$
Coarse	67640	0.3012
Medium	102008	0.3133
Fine	161028	0.3135

the wake region. The computational grid consists of quadrilateral cells with minimum y^+ value of 1 on the duct walls. Standard wall function detailed in Fluent (2011) is used for all the computations. Boundary conditions are: uniform velocity at the inlet, zero gauge static pressure at the outlet, no-slip walls for duct surfaces. A symmetric boundary condition is applied along the center-line axis while a fan boundary condition is used for the AD. To establish yawed inflow conditions, the flow is rotated around the center-line axis by yaw angle α for different test cases. The k-ω SST (shear stress transport) model is used as turbulence model. Preliminary investigations showed good agreement with the experiments (Dighe et al., 2018). The URANS solutions are obtained using the coupled algorithm (Wilcox et al., 1998); it offers robustness and faster convergence as compared to the segregated solution schemes. A least-squares cell-based method is used to evaluate the pressure gradient, with continuity and momentum equations solved using a second order upwind differential scheme. The convergence criteria is set to 10^{-6} for all the residuals. The physical time step corresponding to a Courant- Friedrichs-Lewy (CFL) number of 1 in the finest mesh resolution level, is 1.67×10^{-5} s. A typical converged URANS solution with approximately 0.1 million mesh elements is obtained in roughly 0.5 hour on a multi-core work-station desktop computer.

URANS solutions are dependent on the discretization of the computational domain. Grid independence analysis has been carried out using three grid sizes, where the refinement factor in each direction is approximately 1.5. Refinement factor is defined as the rate at which the grid size increases in the direction normal to the surface of the wall (duct surface). The duct thrust force coefficient $C_{T,D}$ is taken as reference for the convergence analysis. The results of the grid independence study are shown in Table 1. Convergence is reached for the medium refined grid, where the $C_{T,D}$ value fluctuates less than 0.0003%, and similar grid refinement is used in the numerical investigation, hereinafter.

https://doi.org/10.5194/wes-2019-62
Preprint. Discussion started: 5 September 2019

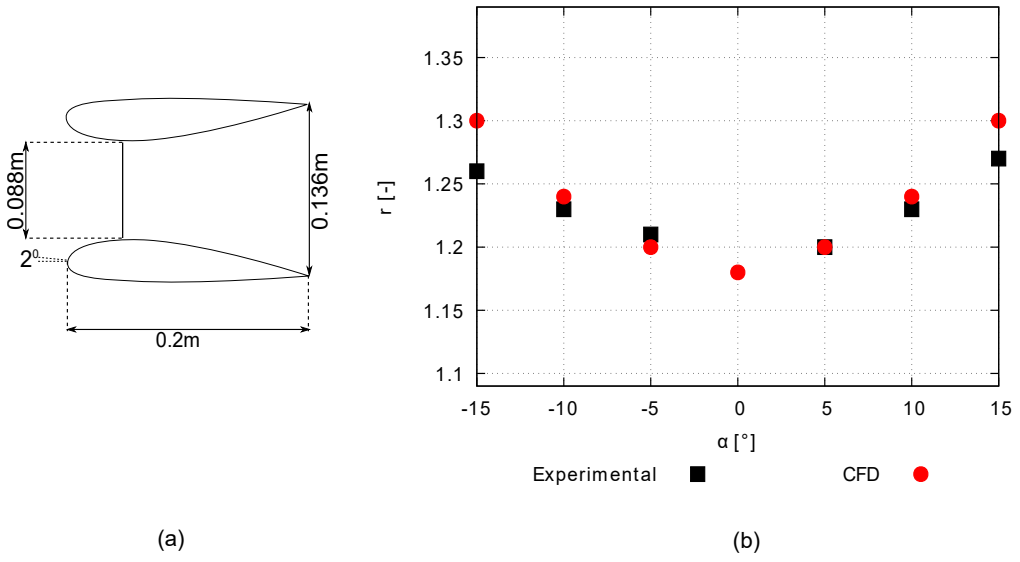

Figure 5. A schematic cross-section layout of the three dimensional experimental model used for the numerical validation study (a), and comparison between experimental findings (Igra, 1981) and the CFD results (b).

4 Numerical validation

For validating the numerical approach, experiments reported by Igra (1981) are simulated. Igra's experiments were conducted in the subsonic wind tunnel of the Israel Aerospace Industry (formerly Israel Aircraft Industry); this tunnel has a large test section and it measures 3.6 m × 2.6 m.

A schematic of the cross-section of the geometry is shown in Figure 5(a). The longitudinal cross-section of the duct is a NACA 4412 airfoil. The leading edge of the duct is rotated by 2° with respect to the free-stream direction, resulting in a duct expansion ratio $\frac{S_e}{S_{AD}}$ = 1.54. The experimental data set consists of: static pressure distribution at different axial and radial positions, and forces generated by the duct surface for a range of flow angles. During the experiments, the inflow velocity was set at U_∞ = 32 m/s. Following Igra (1981), the wall interference and blockage correction can be ignored.

The experimental data is reported in terms of the augmentation factor $r = \frac{C_P}{C_{P_o}}$, which expresses the ratio between the power coefficient of the duct-AD model and the power coefficient of the bare AD model when both the models bear the same AD and similar operating conditions. A good agreement between the CFD simulations and the experimental findings is found in Figure 5(b). The deviation between the CFD and the experimental findings increase with increasing values of α. The maximum deviation is less than 5% for α = 15°. The discrepancies might be due to three-dimensional effects not accounted in the two dimensional simulations. Nevertheless, the trend for r calculated using CFD simulations is similar to that of the experimental findings, thus witnessing the overall trustworthiness of the CFD approach for the scope of the current investigation.

https://doi.org/10.5194/wes-2019-62
Preprint. Discussion started: 5 September 2019

eawe european academy of wind energy
Open Access WIND ENERGY SCIENCE DISCUSSIONS

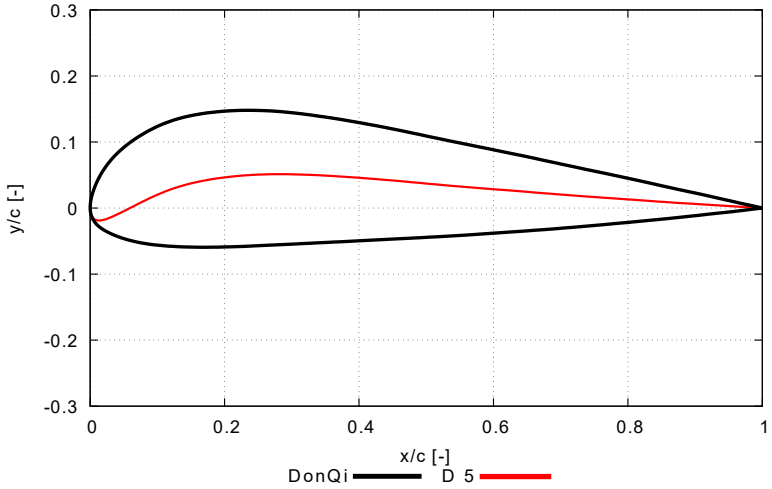

Figure 6. Duct geometries (cross-section) used for the numerical study.

5 Results and Discussion

5.1 Duct geometries

In the following sections, the effects of yaw on the aerodynamic performance of the duct-AD model are quantified. Two duct geometries, shown in Figure 6, with different longitudinal cross section (named as DonQi® and DonQi D5®) are chosen. The selection is based on the duct shape parametrization study conducted by the authors (Dighe et al., 2019). The parametrization procedure for duct shapes preserved the following geometric features: leading edge position (which defines the inlet area ratio), trailing edge position (which defines the exit area ratio) and inner side thickness (which preserves AD radius and clearance). This makes it ideal to isolate the effect of camber on the overall performance. In the study, an optimal $C_{T,AD} = 0.7$ was obtained for both the duct geometries. This value is employed for the rest of the discussion.

5.2 Duct force coefficient

Figure 7 illustrates the variation of duct force coefficient $C_{T,D}$ as a function of yaw angle α obtained for the two duct geometries. $C_{T,D}$ trend-lines are obtained using the results from thirteen simulations ranging from α = 0°-30° in increment of 2.5°. Starting with the trend-line for DonQi® duct, it can be observed that, $C_{T,D}$ decreases with increasing values of α. Conversely, for DonQi D5® duct, $C_{T,D}$ increases with increasing α. A local $C_{T,D}$ maximum at α = 17.5° appears for the DonQi D5® duct. The value of $C_{T,D}$ for DonQi D5® duct decreases for α beyond the local maximum.

The differences in the $C_{T,D}$ trend-lines for the two duct geometries can be explained by looking at the flow-field. Contours of non-dimensional free-stream velocity $\frac{U_x}{U_\infty}$ for both duct geometries are reported in Figures 8 (a) to (h). Four yaw angles, i.e. α = 0°, 10°, 17.5° and 20°, are shown. The contours of DonQi® duct profile show that, with increasing values of α, the magnitude of velocity on the suction side of the duct decreases and the magnitude of velocity on the pressure side of the duct

https://doi.org/10.5194/wes-2019-62
Preprint. Discussion started: 5 September 2019

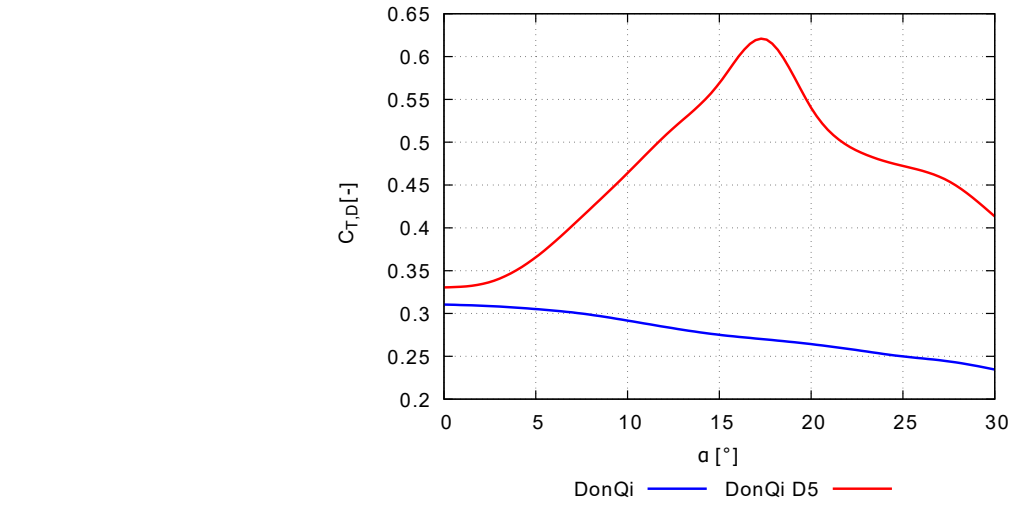

Figure 7. Effect of yawed inflow on the duct thrust force coefficient for the two duct geometries. $C_{T,AD} = 0.7$.

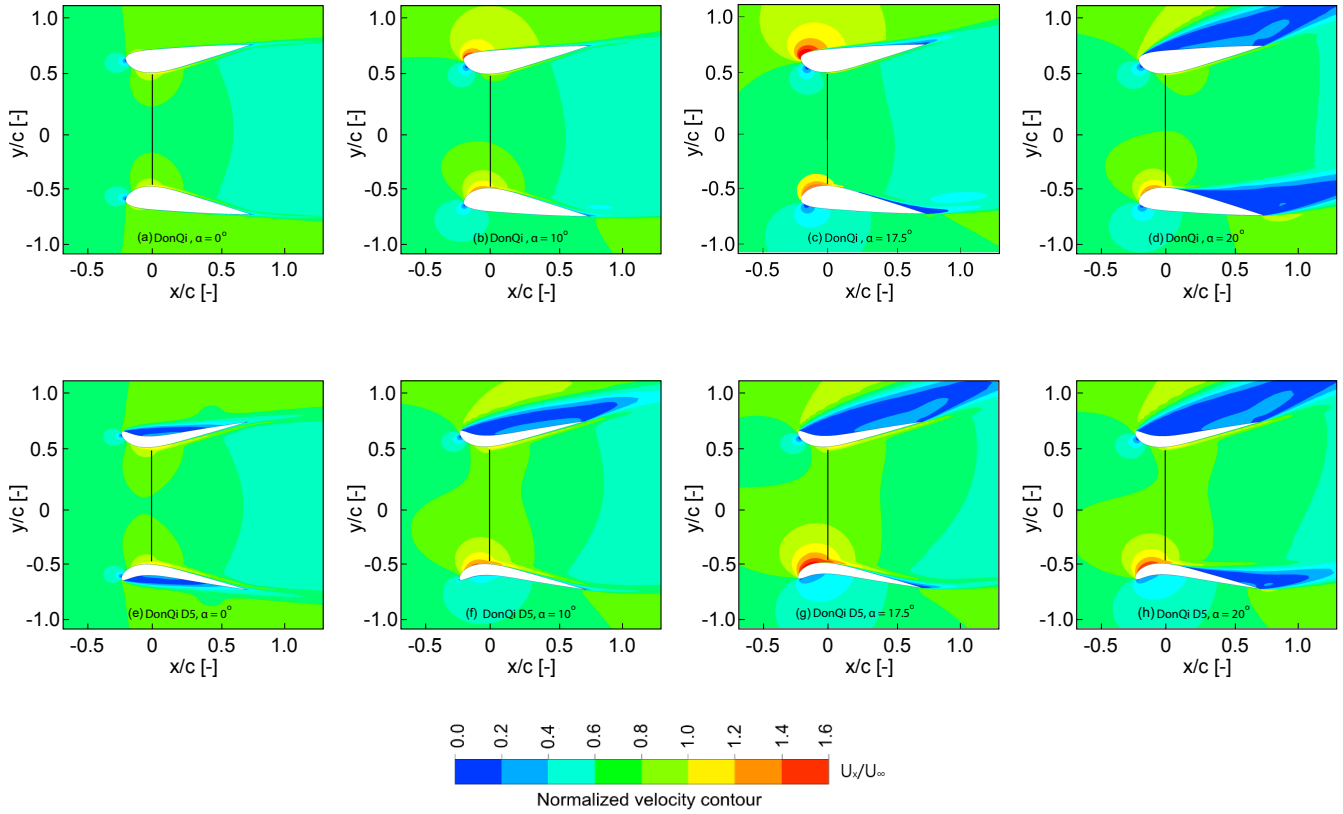

Figure 8. Velocity contours colored with streamwise normalized velocity. The results are depicted for DonQi duct-AD model (top) and DonQi D5 duct-AD model (bottom), both bearing a constant $C_{T,AD} = 0.7$.

https://doi.org/10.5194/wes-2019-62
Preprint. Discussion started: 5 September 2019

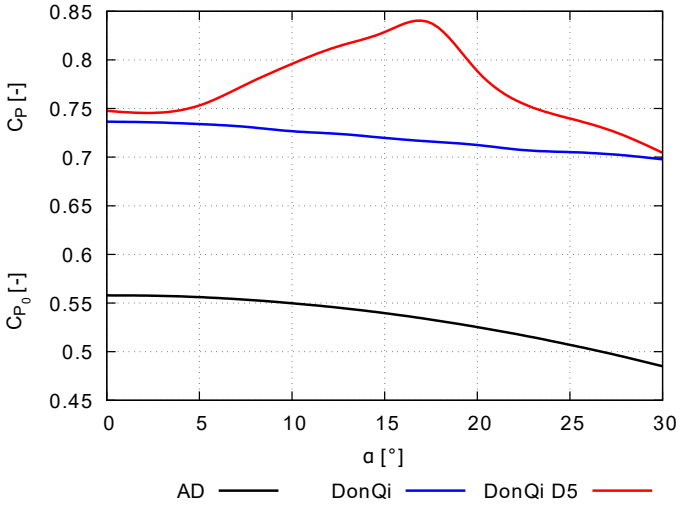

Figure 9. Effect of yawed inflow on the power coefficient.

starts to increase significantly. With the reduced velocity, there is insufficient boundary layer momentum for the flow to remain attached on the suction side of the duct. Subsequently, at α = 20°, the flow is completely detached from the duct surface and the duct has fully stalled. Inner duct wall flow separation is characterized by a strong reduction of duct wall shear stress, and ultimately the reduction of $C_{T,D}$ with increasing values of α in Figure 7. For the DonQi D5® duct, however, increased yaw returns higher velocity magnitude at the suction side of the duct up to α = 17.5°. This is due to the duct profile camber, which promotes flow acceleration on the suction side of the duct. The increased velocity magnitude on the suction side of the duct in this range is always accompanied by flow separation on the pressure side of the duct. As long as the flow separation is limited to the pressure side, the integral of duct thrust force coefficient $C_{T,D}$ in Figure 7 increases up to α = 17.5°. At α = 20°, the flow separation region traverses from the pressure side to the suction side of the duct indicating duct stalling characterized by the reduction of $C_{T,D}$ in Figure 7.

5.3 Power Coefficient

Figure 9 represents the power coefficient C_P, for the two duct configurations, as a function of yaw angle α. For the sake of completeness, C_{P_o} for a bare AD is plotted alongside. The figure shows that, C_P is higher than C_{P_o} for all values of α. Comparing Figures 7 and 9, the C_P trends corresponds with the $C_{T,D}$ trends. The larger the $C_{T,D}$, the higher the C_P reached, and vice-versa. Similar to the $C_{T,D}$ trend for DonQi D5®, maximum $C_P \approx 0.84$ is obtained for the DonQi D5® duct at α = 17.5°; thereafter any further increase in α results in C_P drop.

https://doi.org/10.5194/wes-2019-62
Preprint. Discussion started: 5 September 2019

eawe european academy of wind energy
Open Access WIND ENERGY SCIENCE DISCUSSIONS

6 Conclusions

In this work, the aerodynamic performance of DWT in yawed flow is studied using a simplified duct-AD model. To this aim, two-dimensional numerical calculations using URANS simulations are shown. Based on the existing studies conducted by the authors, two duct geometries with different cross-section camber (named as DonQi® and DonQi D5®) are chosen. To validate the numerical method, the comparison of numerical results with the experimental data are reported. Of the two duct geometries investigated, DonQi D5® duct configuration not only demonstrates an insensitivity to yaw but a gain in the overall performance C_P up to at a yaw angle α = 17.5°. On the contrary, C_P of DonQi® duct configuration drop for $\alpha > 0°$. The C_P gain for the DonQi D5® duct configuration with increasing α corresponds to the dimensionless duct thrust force coefficient $C_{T,D}$, which increases due to the camber effect until the duct stall angle is reached. More precisely, inner duct wall flow separation reduces the $C_{T,D}$ and ultimately the C_P of the DWT model. The ability of DWT to capture power in yawed inflow conditions is potentially beneficial and is the subject of future work.

https://doi.org/10.5194/wes-2019-62
Preprint. Discussion started: 5 September 2019

eawe european academy of wind energy
Open Access WIND ENERGY SCIENCE DISCUSSIONS

Appendix A: Nomenclature

c	Duct chord length $[m]$
C_P	Power coefficient for the duct-AD model [-]
C_{P_0}	Power coefficient for the bare AD [-]
$C_{T,AD}$	AD thrust coefficient [-]
$C_{T,D}$	Duct thrust coefficient [-]
C_T	Total thrust coefficient for the duct-AD model [-]
r	Augmentation factor [-]
S_{AD}	AD reference area $[m^2]$
S_e	Duct exit area $[m^2]$
T_{AD}	AD thrust force $[N]$
T_D	Duct thrust force $[N]$
T	Total thrust force for the duct-AD model $[N]$
U_{AD}	Normalized velocity at the AD plane [m/s]
U_{AD_0}	Normalized velocity for a bare AD [m/s]
U_∞	Free-stream velocity [m/s]
U_x	Stream-wise velocity component across the AD surface [m/s]
x	Variable value vector parallel to the free-stream direction [-]
y	Variable value vector normal to the free-stream direction [-]
α	Inflow yaw angle $[^\circ]$
ρ	Density of air $[kg/m^3]$
∞	Subscript representing quantity evaluated for free-stream condition
AD	Actuator disk
DWT	Ducted wind turbine
$HAWT$	Horizontal axis wind turbine
$LCOE$	Levelized cost of electricity

Author contributions. VVD compiled the literature review, setup the CFD simulations and wrote the bulk of the paper. DS performed the CFD simulations, post-processed the cases and contributed towards writing this paper. FA reviewed the paper and carried out modifications in different sections of this paper. GVB helped formulate the ideas in regular group discussions.

Competing interests. The authors declare that they have no conflict of interest.

https://doi.org/10.5194/wes-2019-62
Preprint. Discussion started: 5 September 2019

Acknowledgements. Authors would like to acknowledge Prof. Ozer Igra for providing the experimental data that have contributed to the part of numerical validation reported in this paper. The research is supported by STW organization, grant number- 12728

https://doi.org/10.5194/wes-2019-62
Preprint. Discussion started: 5 September 2019

eawe european academy of wind energy
Open Access WIND ENERGY SCIENCE DISCUSSIONS

References

Abe, K., Nishida, M., Sakurai, A., Ohya, Y., Kihara, H., Wada, E., and Sato, K.: Experimental and numerical investigations of flow fields behind a small wind turbine with a flanged diffuser, Journal of Wind Engineering and Industrial Aerodynamics, 93, 951–970, 2005.

Bontempo, R. and Manna, M.: Solution of the flow over a non-uniform heavily loaded ducted actuator disk, Journal of Fluid Mechanics, 728, 163–195, 2013.

Dighe, V., de Oliveira, G., Avallone, F., and van Bussel, G.: Towards improving the aerodynamic performance of a ducted wind turbine: A numerical study, in: Journal of Physics: Conference Series, vol. 1037, p. 022016, IOP Publishing, 2018.

Dighe, V., de Oliveira, G., Avallone, F., and van Bussel, G.: Characterization of aerodynamic performance of ducted wind turbines: A numerical study, Wind Energy, 7, 18–422, 2019.

Dupont, E., Koppelaar, R., and Jeanmart, H.: Global available wind energy with physical and energy return on investment constraints, Applied Energy, 209, 322–338, 2018.

Fluent, A.: 14.0 User's Manual, ANSYS Inc., Canonsburg, PA, 2011.

Gielen, D., Boshell, F., Saygin, D., Bazilian, M. D., Wagner, N., and Gorini, R.: The role of renewable energy in the global energy transformation, Energy Strategy Reviews, 24, 38–50, 2019.

Gilbert, B. and Foreman, K.: Experiments with a diffuser-augmented model wind turbine, Journal of Energy Resources Technology, 105, 46–53, 1983.

Igra, O.: Research and development for shrouded wind turbines, Energy Conversion and Management, 21, 13–48, 1981.

Khamlaj, T. and Rumpfkeil, M.: Theoretical Analysis of Shrouded Horizontal Axis Wind Turbines, Energies, 10, 38, 2017.

de Vries, O.: Fluid dynamic aspects of wind energy conversion, Tech. rep., Advisory Group for Aerospace Research and Development NEUILLY-SUR-SEINE (France), 1979.

Phillips, D., Richards, P., and Flay, R.: CFD modelling and the development of the diffuser augmented wind turbine, Wind and Structures, 5, 267–276, 2002.

Tang, J. and van Bussel, G.: Experimental investigation of the aerodynamic interaction between ducts and actuator discs, in: Colloquium on Research and Innovation on Wind Energy on Exploitation in Urban Environment Colloquium, vol. 229, p. 244, Springer, 2018.

Toshimitsu, K., Nishikawa, K., Haruki, W., Oono, S., Takao, M., and Ohya, Y.: PIV measurements of flows around the wind turbines with a flanged-diffuser shroud, Journal of Thermal Science, 17, 375–380, 2008.

van Bussel, G.: The science of making more torque from wind: Diffuser experiments and theory revisited., in: Journal of Physics: Conference Series, vol. 75, p. 012010, IOP Publishing, 2007.

Werle, M. and Presz, W.: Ducted wind/water turbines and propellers revisited, Journal of Propulsion and Power, 24, 1146–1150, 2008.

Wilcox, D. C. et al.: Turbulence modeling for CFD, vol. 2, DCW industries La Canada, CA, 1998.